Mon. Not. R. Astron. Soc. **264,** 497–508 (1993)

Mergers of collisionless systems

F. R. Pearce,[1] P. A. Thomas[1] and H. M. P. Couchman[2]
[1]*Astronomy Centre, Sussex University, Falmer, Brighton BN1 9QH*
[2]*Department of Astronomy, University of Western Ontario, London, Ontario N6A 3KV, Canada*

Accepted 1993 March 20. Received 1993 March 20; in original form 1992 July 20

ABSTRACT

The hierarchical clustering scenario is examined by merging haloes of collisionless particles under controlled conditions. Each simulation contains 16 000 particles, which gives a finer spatial resolution than in previous work. We find that dark matter haloes can grow homologously, obeying simple scaling laws. All the mergers tend towards a single density profile, which in our case closely resembles that given by de Vaucouleurs. The high resolution of our simulations also allows us to look at the resultant core structure of our haloes. We find that the central density is close to the maximum value allowed by phase-space constraints, indicating a smaller core radius in the dark matter than is generally assumed. The expected deviations from our results, given more realistic initial conditions, are discussed.

Key words: methods: numerical – galaxies: clustering – galaxies: formation – dark matter.

1 INTRODUCTION

In this paper we examine the growth of dark haloes in hierarchical clustering scenarios (Press & Schechter 1974). These propose that the structures we currently observe in the Universe, such as galaxies and galaxy clusters, formed via the merger of smaller systems. For a power-law fluctuation spectrum we would expect the distribution and internal structure of dark matter haloes to look the same at all times, merely being scaled to larger sizes and masses as the Universe evolves. Physical processes acting before recombination in the real Universe modify the power spectrum away from a simple power law, and collapsed haloes are not expected to form until $z \approx 100$ or later. So, for the self-similar assumption to be valid, it must be shown that the density profiles of collapsed objects quickly tend to a standard form, early on in the hierarchy, and thereafter scale homologously (during mergers). These problems are investigated in this paper by simulating mergers of haloes with a range of internal structures and collision parameters. We find in favour of the self-similarity hypothesis, with a stable density profile emerging. In our case (finite total mass, vacuum boundary conditions) this profile closely resembles that given by de Vaucouleurs. The trend is for the core size to be reduced relative to that of the halo. We interpret this result as showing that the maximum allowable phase-space density is attained in the core of the new object. The shape of the density profile may depend upon the initial conditions, but we would expect the trend towards self-similarity and the absence of an inner core to remain.

Each halo in our main simulations consists of 8192 particles, smoothly distributed in phase space. To keep the model simple, we ignore subcondensations so that the effects of two-body relaxation and dynamical friction are eliminated as much as possible. This will be a good approximation in galaxies, where the time-scales for these processes are known to be large, and also in clusters, if galaxies contain a small fraction of the total mass as is suggested by theoretical models (see e.g. Merritt 1988).

There are three ways in which N-body simulations have been used to investigate the density profiles of collapsed objects. The first is to study the isolated collapse of an overdense region, looking at its final density profile after a few crossing times (van Albada 1982; May & van Albada 1984; Aquilar & Merritt 1990; Katz 1991; Londrillo, Messina & Stiavelli 1991). These simulations show that a $\rho \propto r^{-3}$ profile is produced from almost all 'cold' initial conditions in which the random kinetic energy is much less than the potential energy and which involve large collapse factors. Unfortunately, by the time the major merger event takes place, the precursor density profile and phase-space distribution are rather chaotic. Others (White 1978, 1979, 1980; Villumsen 1982, 1983) have looked at galaxy-galaxy mergers, but the limited number of particles (250 for White, 600 for Villumsen) gives poor resolution in the inner regions. This method seems to have been neglected in recent years (although the simulations of Katz and van Albada mentioned above often do involve the merger of two similarly sized objects). This merging approach is the method used for the simulations presented in this paper, with the well-defined initial condi-

tions allowing detailed analysis. The most realistic simulations evolve a section of the Universe with an imposed structure (usually a set of Gaussian fluctuations), and then look at a small region representing a cluster (Cavaliere et al. 1986; Quinn, Salmon & Zurek 1986; West, Dekel & Oemler 1987; Efstathiou et al. 1988; Evrard 1990; Thomas & Couchman 1992; Warren et al. 1992). These simulations give a more accurate representation of the initial fluctuations, tidal forces and subsequent infall expected in a more realistic model, but the large density contrasts involved in this approach (only 5 per cent of galaxies are in rich clusters) lead again to a restricted number of particles in the interesting central region.

We find in our simulations that mergers do tend to produce a unique density profile with $\rho \propto r^{-3}$ throughout the bulk of the halo. The degree of variation about this typical end-state is small. A density slope of -3, which gives divergent mass to both small and large radii, is perhaps the natural one to expect. It is a common result in the above-mentioned papers and, with a modest steepening at large radii and flattening at small radii, it closely resembles the ubiquitous de Vaucouleurs profile. It should be noted that the third class of simulation with realistic initial conditions tends to give more extended profiles with slopes closer to -2. This will be discussed further in Section 4.2.

We are especially interested in whether there is a core radius in the density distribution of the dark matter. Is there some radius within which the density tends to a constant value, or does the density profile rise without a break into the very central regions? In a true homology there exists only a single effective radius. This is true of the de Vaucouleurs profile but not of $\rho \propto r^{-s}$, where $0 < s \leq 3$, which must have an outer cut-off to prevent mass divergence as well as an inner core radius to give a finite central density. There seems to be no physical reason why these two radii should scale in the same manner. The outer radius is determined by mass conservation, whereas the inner one (in the absence of dissipation) may be a phase-space density limitation.

In all the simulations carried out so far, the restricted number of particles has led to a lack of information about the central regions. Every approach requires a short-range softening in the force law to prevent two-body relaxation effects. With only a few particles, this softening length, within which scattering effects are reduced, is large (see Thomas & Couchman 1992 for a fuller discussion). Clumps of matter cannot form on scales less than the softening length, forcing constant-density cores. This has been generally recognized, and many previous authors (e.g. White 1978; Villumsen 1982; Katz 1991) point out that nothing useful can be inferred from the behaviour of the central regions in their simulations. In this paper we use sufficient numbers of particles that we can resolve the core regions and investigate their evolution in mergers. We find in every case that the core shrinks by close to the maximum amount allowed by phase-space constraints, and therefore in an extended hierarchy can be regarded as having zero radius. In other words, models with only one effective radius, fixed by the total mass, fit the data better than those with an additional inner core radius.

In this paper we take simple halo models, similar to those used by White (1978), and collide them with a range of speeds and impact parameters. By using such basic models, we hope to understand what is actually going on during the merger, as the initial phase-space distribution is well understood. The greater number of particles used (at least 8192 per initial cluster) allows greater resolution than previously achieved, pushing the smoothing length within the expected core radius. In Section 2 we give the initial conditions for the simulations, detail the code used and show the results of several tests. In Section 3 we present the results of the simulations and discuss the emergence of a homology. Finally, Section 4 contains a summary and a more wide-ranging discussion of the results.

2 METHOD

2.1 Code

Most of the runs described in this paper were carried out using an adaptive particle-particle, particle-mesh (AdP^{3}M) code developed by one of us (Couchman 1991). This is a major advance on previous mesh schemes, as it automatically provides extra resolution in the denser regions, allowing greater density contrasts to be followed in a reasonable amount of time. Mesh codes utilize either vacuum or wrapped boundary conditions at the edge of the box. Wrapped conditions, where particles leaving one side of the box 'appear' on the opposite side and the potential is calculated by assuming that the box repeats itself, are usual in cosmological applications. Here we follow an isolated merger, and so vacuum boundary conditions are used. Particles hitting the edge of the box are assumed to be escaping, and are removed from the simulation. The initial size of the haloes is taken to be a quarter that of the box, so that very few particles escape and those that do so have a negligible effect on the final structure.

We also have a version of Lars Hernquist's TREECODE (Hernquist 1987), running on identical data sets. This code is slower, but it provides a useful check of the method because of the fundamentally different approach employed (Barnes & Hut 1986). Tests of the individual codes used have been published elsewhere (Hernquist 1987; Couchman 1991).

2.2 Initial conditions

In the majority of our runs, the haloes each consist of 8192 particles. This gives adequate resolution with a reasonable speed. Some 'secondary' starting conditions use the output of previous 'primary' runs: these have slightly more particles. Finally, there are a couple of runs with different numbers of particles to check for the unwanted effect of relaxation.

Most of the systems we model have initial density profiles

$$\rho = \rho_c \left[1 + \left(\frac{r}{r_c} \right)^2 \right]^{-s/2} \qquad (1)$$

within some outer radius R_{max}; $\rho = 0$ beyond R_{max}. Here ρ_c is the central density and r_c is the cluster core radius. s defines the slope of the profile outside the core, with $s = 3$ giving the Hubble profile, similar to a King model (King 1966) of central concentration (tidal radius/core radius) 10.9 in the inner regions. Clusters with $s = 2$ are more extended than this, being the end-point of complete virial relaxation, and have a lower central density for a fixed outer radius and total mass.

All the mergers were started with the two clusters separated by their combined maximum radii along the collision axis. For head-on encounters, this corresponds to them just touching. Any offset was then applied in a direction perpendicular to the collision axis. The collision velocity was set equal to either the circular speed at the edge of one of the major clouds or twice this value. This gives the same initial collision velocities for all of the runs. This choice of initial conditions produces a bound system, with binding energies similar to those expected for objects on the scale of clusters (see below).

The core radius needs to be well within the outer boundary, but large enough so that we can detect a reduction during mergers. We compromise on $R_{\max}/r_c = 16$ in our primary simulations. The gravitational softening was fixed at $r_s = 0.4r_c$, above the interparticle separation in the original cores. This is large enough that the numerical effects, discussed in Section 2.4, are not a problem.

The time-step, Δt, in our simulations is fixed by the condition

$$\Delta t = 0.25 \min_i \left(\frac{r_s}{a_i}\right)^{1/2}, \qquad (2)$$

where a_i is the acceleration on particle i. We should really use the local particle separation rather than the smoothing length, r_s, in this expression. However, this would lead to short time-steps in the centrally condensed models. This choice leads to a small nett energy gain in the $s=4$ case, which will tend to puff up the core. However, the time-scale on which this happens is much longer than that of our simulation. We have verified that the core structure in an isolated $s=4$ halo is essentially unchanged after 40 crossing times. Use of the correct time-step condition would slow the code by a factor r_s/b, where b is the smallest interparticle separation (about 7 in the $s=4$ case).

Once a density profile has been selected, there are several sensible ways of choosing the velocity distribution. In real clusters we expect the central regions to be virialized with particles on isotropic orbits, whereas in the outer regions continuing infall will lead to predominantly radial orbits. We would like to choose a velocity distribution that maintains the density profile, so that any observed changes are entirely due to the collision. Following White (1978), we initially chose to use two forms of velocity distribution. One consists of White's 'circ.' configuration, where all the particles initially move on circular orbits. This is not a very physical set-up, but it gives the minimum mixing of particles at different radii. We denote these runs 'circular', and label them by the prefix c. A second approach is White's 'iso.' configuration, where the particles initially have an isotropic velocity distribution, with the initial speed equivalent to the circular speed at that radius. Unfortunately, this does not give a static configuration, although it is not far removed from one. Much greater mixing between particles at different radii now occurs, and this is closer to the expected final velocity distribution in the central regions. However, neither of the above configurations is suitable for looking at the growth of cores, as they do not adequately fill the available phase space. We also therefore generated static initial models with isotropic orbits which satisfied the spherically symmetric Jeans equation (Binney & Tremaine 1987, equation 4-54), given the appropriate density profile (ignoring the outer cut-off). These we call 'full' initial conditions, and we label them with the prefix f. The particle velocities are set equal to the three-dimensional velocity dispersion derived from the Jeans equation oriented randomly. The complete list of initial conditions is given in Table 1.

2.3 Tests

We ran top-hat collapses (constant-density spheres with no initial kinetic energy) and checked the density evolution against the theoretical curve, demonstrating that both the codes were correctly implemented on our system. Collapse factors of 30 were successfully modelled with energy conservation better than 1 per cent. At maximum compression, departures from spherical symmetry are evident in the TREE code, which indicate a directional force dependence. This is not apparent in the AdP^{3}M runs.

Before colliding two model clusters together, we tested our system initialization algorithm by checking that the supposedly stable initial configurations remained static. The density profiles remained constant (within statistical fluctuations) over periods longer than those modelled during the mergers that follow (several crossing times). The total system potential and kinetic energy (and therefore the total energy) was conserved to better than 1 per cent in this test.

During a collision, the simplest way to follow the evolution of the system is to look at the total kinetic and potential energy. A typical plot is given as Fig. 1, scaled so that the gravitational constant, G, the total initial mass, M, of both haloes and their outer radii, $R_{\max}$, are all equal to unity. The time unit is taken to be $(R_{\max}^3/GM)^{1/2}$. For the finite volume of AdP^{3}M, some particles will cross the boundary of the box. These are removed from the simulation, as they are assumed to be escaping, with the lost kinetic and potential energy being remembered and included in the plot. This lost energy is always small, as most of the potential escapers (particles with positive total energy) are still within the simulated box at the end of the runs. Total energy is conserved to about 2 per cent in the $s=2$ and $s=3$ cases, but is slightly worse in the more centrally condensed $s=4$ case because of the large time-step, producing a systematic drift in the total energy to higher values, and a small jump in the total energy on each close approach. Bounces can clearly be distinguished in Fig. 1, with the system going through two distinct oscillations before settling towards a steady state.

The main aim of this paper is to look at the density profiles of the post-merger objects. Care needs to be taken, as the core structure shown in the density profile is highly sensitive to the position chosen for the centre. This effect has already been stressed for observational fitting of galaxy density profiles to number counts in galaxy clusters, where a spurious core radius can be introduced if the fitting centre is offset from the true centre (Beers & Tonry 1986; Merrifield & Kent 1989). Several algorithms have been suggested for finding the true centre; these divide into two main approaches. The first uses the median or the centre-of-mass of particles within a given distance, d, of the guessed centre whose position is then iterated to find a self-consistent solution. The problem with this method is that if d is small then the region will have approximately constant density and the centre will be ill-defined, whereas if d is large then the signal

Table 1. All of the runs mentioned in the text, grouped into similar types. The first column contains a run identifier, where the number corresponds to the slope, s, of the original haloes; f and c denote whether the initial velocities were isotropic or circular; an s indicates a second merger, and o signifies an offset collision. The second and third columns give the core radius and slope of a best-fitting King model. The fourth column lists the slope at the half-mass radius, listed in column 8. Column 5 shows the range over which the de Vaucouleurs profile fits the data. Most of the fits were made by fixing $r_e = 0.77 r_{0.5}$, leaving the amplitude as the only free parameter. The next two columns list f_m and f_e, defined in the text, which are required to test the derived scaling relations. The predicted half-mass radius, r_p, is given in the final column.

Name	R_c	s	S	deV range	f_m	f_e	$r_{0.5}$	r_p
individual halos								
2	2.5	2.0	2.0		---	---	22.	---
3	2.5	3.0	3.0		---	---	11.	---
4	2.5	4.0	4.0		---	---	5.1	---
'full' initial velocities								
f2	2.3	2.3	3.0	5.0–80.	1.00	1.40	34.	31.
f3	**2.2**	**2.8**	**3.0**	2.5–32.	1.00	1.17	20.	19.
f4	2.0	3.6	3.2	2.0–28.†	0.97	1.08	9.3	8.9
secondary runs								
f2s	3.3	2.6	2.7	1.8–21.†	1.00	1.46	32.	30.
f3s	2.8	3.0	3.0	3.0–55.	1.00	1.32	23.	22.
f4s	1.6	3.1	2.8	1.5–25.	0.99	1.15	13.	11.
'circular' initial velocities								
c2	0.4*	1.8*	2.7	0.5–27.†	0.99	1.30	27.	33.
c3	1.0	2.5	3.0	1.0–38.	0.97	1.17	19.	18.
c4	0.9	3.0	3.1	1.0–30.†	0.96	1.09	10.	8.6
offset runs								
f3o	2.2	2.8	2.9	3.0–40.	1.00	1.16	20.	19.
c3o	0.8	2.5	3.0	1.0–30.	0.98	1.16	20.	19.
various test runs								
f3small	0.3	2.2	3.0		0.99	1.17	18.	19.
f3large	2.0	2.7	2.9		0.98	1.18	21.	19.
f3mass	3.0	3.1	3.1		1.00	1.17	20.	19.
f3slow	2.2	2.8	2.7		1.00	1.31	18.	17.
f3fast	2.3	3.0	3.2		1.00	0.64	34.	35.

*Notes: poor fit; † $r_e \neq 0.77 r_{0.5}$.

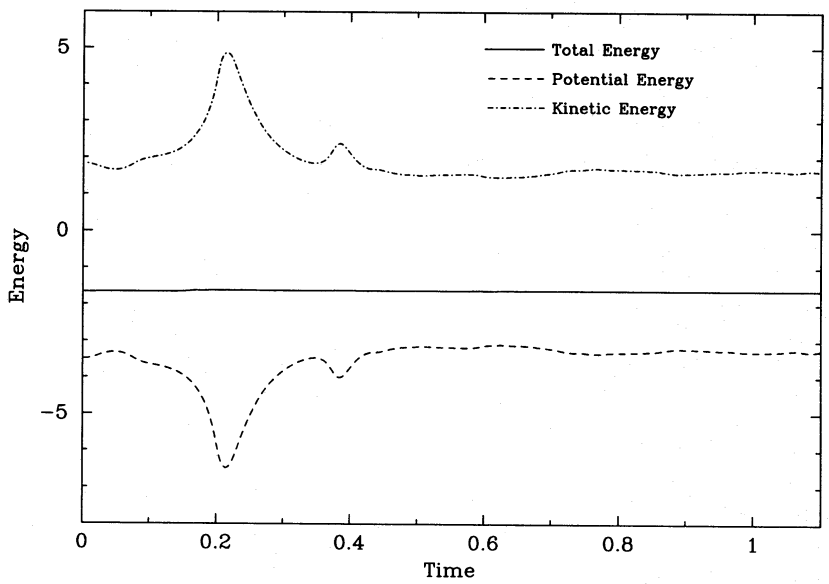

Figure 1. Energy plot from the f3 merger. The energy is in units of the total initial mass, the maximum radius of one of the initial clusters (R_{max}) and $G = 1$. The time unit is taken to be $(R^3_{max}/GM)^{1/2}$. Two distinct 'bounces' can be seen, and the long 'run out' required for the final object to settle down.

is dominated by distant particles which may not be symmetrically distributed or even be bound to the system. The alternative approach is to use the binding energy of individual particles, with the most tightly bound particle being used to define the centre of the object. This approach seems to work very well, and it invariably gives smaller core radii than the centroid method. We also tried taking the centroid of the 500 or so most tightly bound particles, so as not to rely on a single particle. This gives essentially identical results and was used as a simple check upon the single most tightly bound particle method, which is the one adopted in this paper.

Radial profiles are generated by binning the particles in spherical shells around the most bound particle. A typical density profile obtained in this manner is shown in Fig. 2, along with the initial density profile of one of the merging clusters.

Different projections of phase space provide useful diagnostics of the state of the system. One of the simplest is a radial velocity versus radius plot (Fig. 3). This shows where streaming is occurring (obvious in the outer regions), and indicates to what radius the density profile has settled into a steady state. The energy (kinetic + potential) versus radius plot (Fig. 4) often displays obvious phase wrapping (seen

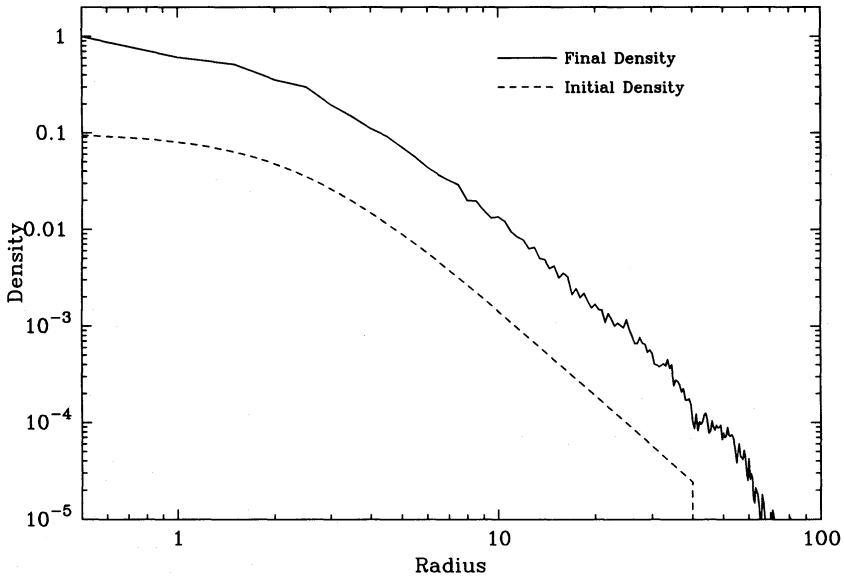

Figure 2. Density profile for the end-state of run f3, scaled in units of the central density, along with the profile of the initial objects, scaled arbitrarily to 0.1. Radius is the distance from the most tightly bound particle in units of the softening length, r_s.

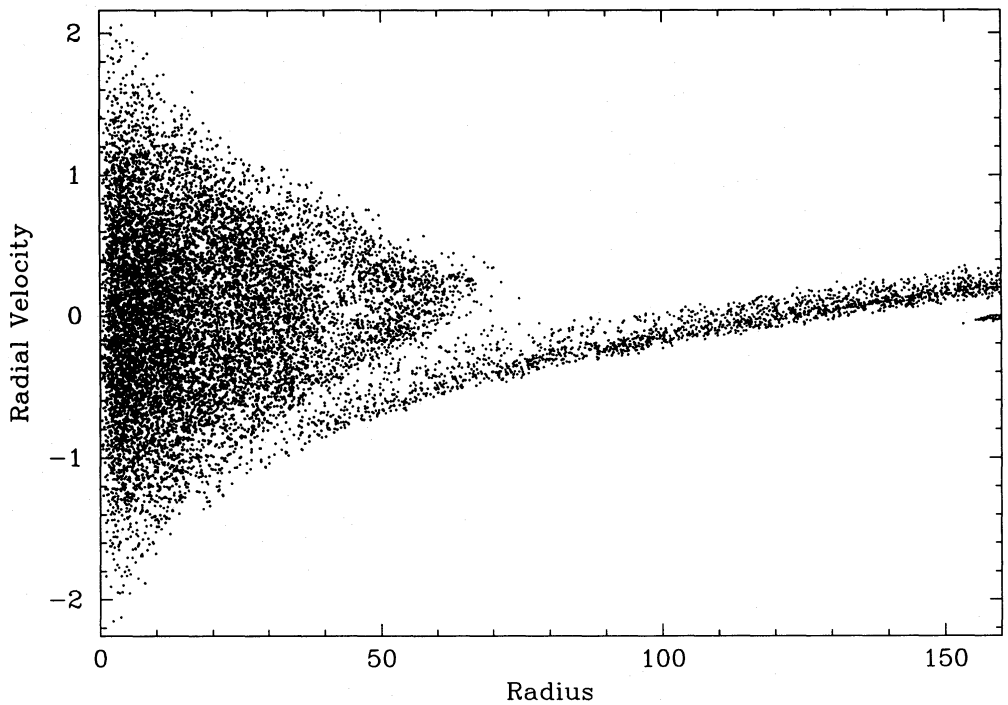

Figure 3. Phase-space plot of the radius, again in units of r_s, against the radial velocity, scaled to the central three-dimensional velocity dispersion of an initial object.

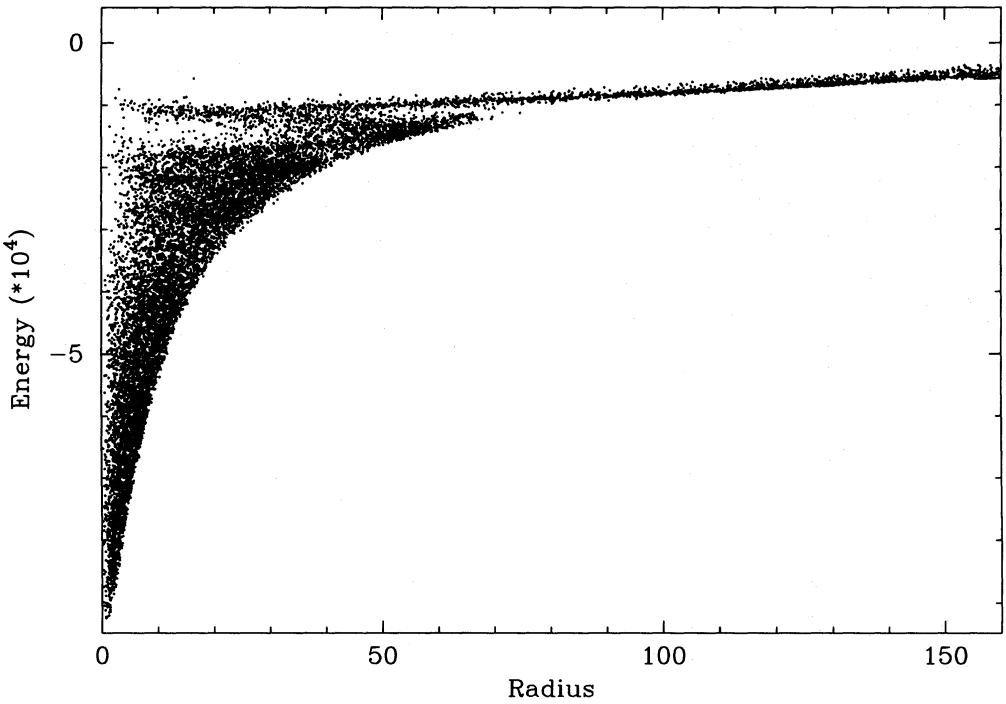

Figure 4. Radius in units of r_s plotted against the total energy of each particle, in the energy units of Fig. 1.

towards the top). The sharp boundaries of the densely populated regions of phase space indicate that little local scattering of particles has occurred.

2.4 Numerical effects

In our merger simulations, there are two relaxation processes which redistribute the particles in phase space. Violent relaxation is a physical effect, whilst two-body relaxation is an unwanted side-effect of using an N-body simulation with only a small number of particles. In the former case, particle energies alter because of the fluctuating potential during the merger; in the latter, it is interactions between pairs of particles that are important. Because of this, two-body relaxation need not preserve phase-space density along particle trajectories, and can lead to an artificial reduction in the core radius. These two processes can be distinguished, because in violent relaxation all masses are affected in the same way, whereas in two-body relaxation high-mass particles tend to lose energy to low-mass ones by a process known as dynamical friction (i.e. the system tends towards equipartition of energy).

The relaxation time, t_r, at the centre of the halo can be estimated by rewriting equation (13) of Thomas & Couchman (1992) as

$$t_r \sim \frac{27N_c}{8\ln(r_c/r_s)}\frac{r_c}{R_{max}}t_d, \qquad (3)$$

where N_c is the number of particles in the core, and $t_d = R_{max}/v$ (where v is a typical velocity) is the crossing or dynamical time. Putting in the appropriate values gives $t_r \sim 0.23N_c t_d$, which is much greater than unity as even the most extended profile ($s=2$) has $N_c > 100$. This remains true for smaller cores, because two-body relaxation rapidly becomes ineffective on scales close to the smoothing length. We therefore expect numerical relaxation to be unimportant in our simulations.

To test this conclusion, we conducted three test runs. Each resembled run f3, apart from one factor. The first run, f3large, had four times as many (32768) particles in each halo, while the second, f3small, had only one-quarter as many (2048) particles. A third run, f3mass, had a range of particle masses. We also compared the results of the TREE code f3 run with that using AdP^{3}M: the two are essentially identical.

The results from f3large are very similar to those obtained from f3, with only small statistical differences. However, f3small displays the signature of two-body relaxation in the centre, where the density profile continues to rise with slope -2. The density profiles for these runs are compared with the profile obtained with 8192 particles in Fig. 5.

In run f3mass every third particle had mass 2 units, and the others mass $\frac{1}{2}$, giving the same total mass as before. In this heterogenous system, the heavy particles act as more efficient scatterers, and the relaxation time-scale is reduced by a factor of about 1.5. This is also the time-scale for energy transfer between the two particle types. The density profiles of each are nearly indistinguishable. Careful examination of an energy histogram reveals that the most tightly bound (most slowly moving) mass-2 particles have slightly increased in number, and this is reflected as an excess of heavy particles near to the centre. The effect is only small, however, and is confined to within the smoothing length. Outside this radius the two distributions are indistinguishable.

We conclude that numerical relaxation is not important in our simulations.

3 RESULTS

Table 1 lists all the merger simulations that we carried out, together with some diagnostic information about the result-

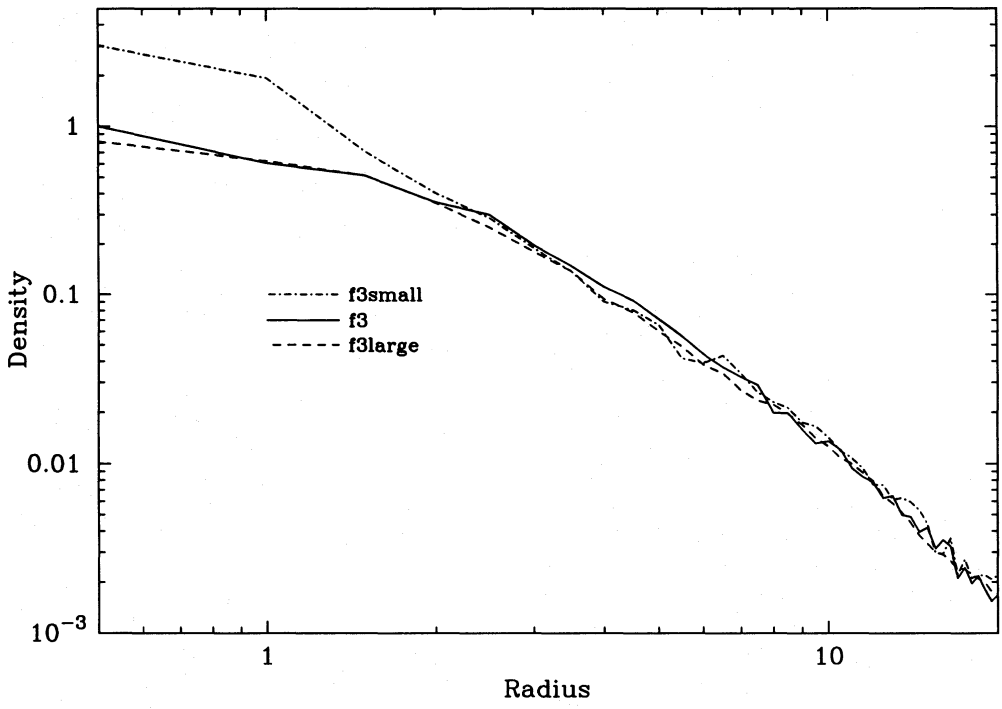

Figure 5. Density profiles for runs f3small, f3large and f3. The densities are all scaled so that the central density of run f3 is unity.

ant object. During every collision a standard sequence of events takes place. The clusters approach until they overlap completely, with the depth of the potential energy dip (or spike if the potential energy is inverted as in Fig. 6) depending on the degree of central concentration in the original clusters. The clusters pass through this overlap and re-separate noticeably. In some cases, three distinct minima in the potential energy can be distinguished, indicating several 'bounces'. The more centrally concentrated clusters have deeper potential energy minima and relax more efficiently, so that they spend less time between bounces.

Each of the runs was followed for several crossing times until a steady state had developed in the central regions (i.e. changes are occurring only on the much longer two-body relaxation time-scale). Streaming motions of entire shells of particles are evident in the outer regions, where few crossing times have elapsed (see Fig. 3, a typical phase-space plot). In most of our runs the initial system is bound; a small number of particles do escape, but these carry little energy with them.

Our primary runs start with density profiles of the form given in equation (1). We also fit this functional form to the merger product, and the results are given in Table 1. These fits are generally very good in the centre, within the quarter- to half-mass radius. The core radius, r_c, is formally accurate to within ± 0.1 times the softening length, r_s, but uncertainties in the position of the centre can increase r_c by up to about $0.2r_s$. The error in s is about ± 0.1, depending upon the extent of the region being fitted. In most cases the density profile 'rolls over', i.e. the slope steepens as the radius increases: we fit a power law, $\rho \propto r^{-S}$, to the density profile at the half-mass radius to give some indication of the break in the slope. Typical variations in S are ± 0.2. In the outer regions the slope must exceed 3 for the total mass to be finite. Usually we see a sharp cut-off at the outer edge of the virialized region of the merger product.

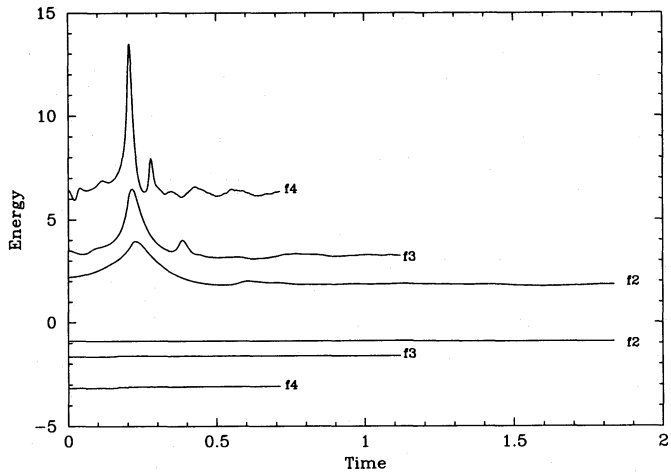

Figure 6. Energy plots from runs f2, f3 and f4. The kinetic energy is omitted, with only the total energy and minus the potential energy being shown for clarity. The units are those of Fig. 1.

For two identical isolated haloes that are just bound, the total mass and energy are just twice the individual values. In fact, some particles will be lost in the collision, and the orbital energy will not be exactly zero. We define two characteristic parameters of the homology:

$$f_m = \frac{m_f}{2m_i} = \frac{2m_i - m_e}{2m_i}$$

and (4)

$$f_e = \frac{e_f}{2e_i} = \frac{2e_i + e_b - e_e}{2e_i},$$

where the subscripts i, f and e refer to each initial halo, to the final merged halo, and to the escaping particles, respectively, and e_b is the initial orbital binding energy. We will use f_m and f_e in the following discussion to derive simple scaling laws for the homology.

3.1 Evolution of the core

The most obvious result from Table 1 is that the circular runs have small core radii in the final state, at or below the softening length, $r_c \lesssim r_s$, whereas the full runs have cores that are only slightly less than in the initial profiles, $r_c \approx 2.5 r_s$. The reason for this difference lies in the occupation of phase space by the initial particle motions. The full initial conditions effectively fill two of the phase-space velocity dimensions initially, and some spread occurs into the third by the time the collision takes place, as the distribution function is not static. The velocities in the circular runs, however, are initially tangential to the radial direction in the halo and remain confined to a single velocity dimension, as they do have a static distribution function. Now, in any collisionless system, the (coarse-grained) phase-space density following particle motions can only decrease (this is analogous to the increase of entropy in dissipational systems), and this limits the allowed size of the final core for the full runs, whereas in the circular simulations the core shrinks to the softening length.

The central phase-space density, Ξ_c, is proportional to $\rho_c \sigma_c^{-3}$, where the subscript c refers to core values. For most smooth profiles, σ is only a slow function of position, and so it is reasonable to take $\rho_c r_c^2 \propto \sigma_c^2 \propto \sigma^2 \propto e/m$, where e is the total energy and m the total mass. Then $\Xi_c \propto r_c^{-2}\sigma^{-1} \propto r_c^{-2}(e/m)^{-1/2}$. The condition $\Xi_f \leq \Xi_i$ thus implies that $r_{cf} \geq (f_m/f_e)^{-1/4} r_{ci}$. Putting in typical values, $f_m \approx 1$ and $f_e \approx 1.2$, we find that the initial and final core radii are related by $r_{cf} \gtrsim 0.96 r_{ci}$. Thus the core radius can decrease only slightly on each merger. In fact, the decreases shown in Table 1 for the full runs are slightly larger than this, because their evolution is not exactly self-similar. In each case the central phase-space density attained is very close to that in the initial haloes. Even though the core radius changes very little, the ratio of the core radius to the half-mass radius does decrease substantially. This suggests that on each collision the core will become smaller.

To test the robustness of this conclusion we performed some off-centre collisions. We tried many different runs, and they all behave in the same way as those reported in Table 1. These were each offset in a direction perpendicular to the collision axis by $40 r_s$, i.e. a quarter of the initial separation of centres. If the haloes were point masses, this would correspond to a minimum separation of $r_c = 2.5 r_s$: in fact, because of the large degree of interpenetration, the minimum separation of centres (assuming each halo moved as a solid body) would be larger than this. The systemic angular momentum, J, expressed in the dimensionless combination $J|\Omega|^{1/2}/GM^{5/2}$ is equal to 0.08 and 0.09 for runs f3o and c3o, respectively, which is much larger than predicted by theoretical calculations and numerical simulations of the acquisition of angular momentum by tidal torques in the early Universe (see e.g. Quinn & Binney 1992). The offset makes no observable difference to the final density profiles of the objects. The mean rotation velocity of spherical shells is approximately independent of radius in the circular case, but increases outwards for the full runs.

In conclusion, a second characteristic radius, the inner core radius, does not seem to be required. Phase-space arguments allow it to decrease at each stage of the hierarchy, and our simulations suggest that this does indeed occur. Where there is no phase-space constraint, i.e. in our circular runs, the core shrinks to the softening length in one encounter.

3.2 Homology?

The results from Table 1 show that steep profiles become flatter and flat ones steepen. The initial slopes of the full runs, {2,3,4}, become $s = \{2.3, 2.8, 3.6\}$ and $S = \{3.0, 3.0, 3.2\}$. In other words, the profiles tend towards a restricted range of end-states. The circular runs show a similar behaviour, with final slopes $s = \{1.8, 2.5, 3.0\}$ and $S = \{2.7, 3.0, 3.1\}$. The final density profiles of the full runs are shown in Fig. 7, bounded by the initial profiles of the $s = 2$ and $s = 4$ cases. The trend is towards the central $s = 3$ profile. In Fig. 8 the final density profiles for the circular runs are shown, scaled in the same way as Fig. 7. The lack of a phase-space limitation in the centre allows much higher central densities in these cases.

To check whether this convergence of density profiles continues, we performed some secondary simulations in which the inner regions of the end-states of the full runs were used as initial conditions for a further merger. All the particles within $40 r_s$ of the centre were used in the $s = 4$ case, all those within $80 r_s$ for $s = 2$ and 3. There are then about 12 000 particles in each new halo, as the outer regions (where large streaming motions persist) have been removed. The half-mass radii for these precursors were 22, 14.5 and $6.7 r_s$ for $s = 2, 3, 4$ respectively. In each case, one of the haloes was rotated through 90° before collision to prevent the growth of anisotropy along the merger axis. This time the range of slopes is even smaller, with $s = \{2.6, 3.0, 3.1\}$. The ratio of the core radius to the half-mass radius continues to drop in all cases.

It can be seen from the difference between s and S that the profiles are not described by a pure power law outside the core radius. The inner slope s is influenced by the core structure but appears to settle down to values in the range 2.6–3.1, whereas S, the slope at the half-mass radius, is typically about 3. Beyond this radius, all the profiles become even steeper (see Figs 7 and 8). For reasons discussed in the previous section, we believe that the runs without a discernible core radius define the true homology. Accordingly, we look for density models with a single radial parameter to fit the data. The most obvious of these is the de Vaucouleurs $r^{1/4}$ law, which has been extensively tabulated by Young (1976). An asymptotic approximation to the density profile is

$$\rho \propto \frac{\exp(-bj)}{2j^3}\left(\frac{\pi}{8bj}\right)^{1/2}, \qquad (5)$$

where $b \approx 7.67$ and $j = (r/r_e)^{1/4}$. Here r_e is the 'effective radius', containing half the projected mass. It is related to the half-mass radius (the radius of a sphere containing half the mass) by $r_{0.5} \approx 1.30 r_e$. This approximation is valid for $j \gtrsim 0.4$, i.e. $r \gtrsim 0.026 r_e$. The de Vaucouleurs profile has a density slope at the half-mass radius of $S = 2.9$, which is similar to the values listed in Table 1.

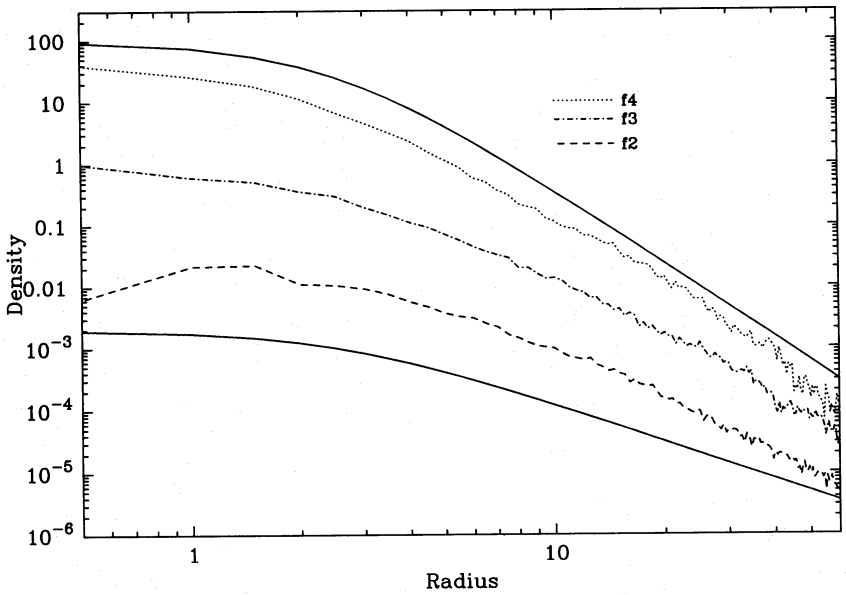

Figure 7. The final density profiles from runs f2, f3 and f4, scaled by one decade around f3. The initial density profiles for the f4 and f2 runs lie above and below respectively. The f4 profile has become shallower, whilst the f2 profile is steeper.

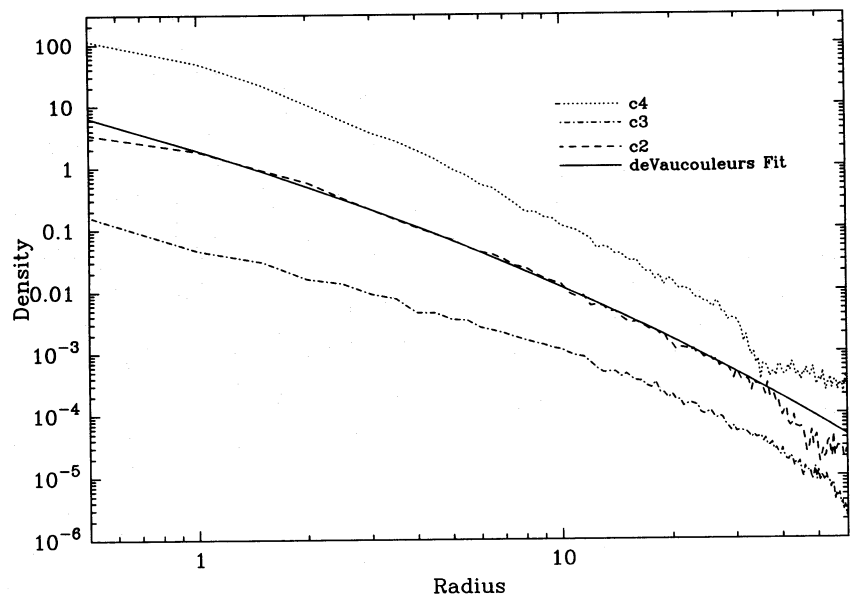

Figure 8. The final density profiles for runs c2, c3 and c4. They are all scaled to the central density of run f3, which is taken to be unity, with the profiles for c4 and c2 being scaled up and down by one decade respectively. The de Vaucouleurs fit to run c3 is shown.

We find that the de Vaucouleurs profile is often a good fit near the half-mass radius. Column 5 of Table 1 gives the range of radii for which the de Vaucouleurs fit is acceptable. In most cases r_e was fixed at $0.77r_{0.5}$, leaving the amplitude as the only free parameter. Remarkably good fits were still obtained in the majority of cases, but for some of the centrally condensed $s=4$ runs a lower r_e is required, whilst some of the more extended $s=2$ runs require a higher r_e. This may indicate that the homology takes more than one collision to establish itself fully. The run c3 gives the best fit over a wide range of radii (see Fig. 8), and the de Vaucouleurs fit is clearly much better than a King model (equation 1) in this case. It is thus reasonable to suppose that something resembling a de Vaucouleurs model is the desired homologue.

The simulations described so far all have the same initial orbital kinetic energy. We also performed a couple of other simulations, one with half and the other with twice the usual collision speed (f3slow and f3fast, respectively). The latter has positive orbital energy (i.e. if the haloes were point masses it would be unbound) but negative total energy. These simulations give end-states that differ by a factor of 2 in scale, and yet they have very similar density profiles.

The merger products are not isotropic but are in general extended along the collision direction. The ellipticity depends upon the initial s and upon the speed of collision,

being largest for f3fast. Subsequent mergers along the same axis can increase the ellipticity still further, whereas collisions in other directions just maintain a small nett anisotropy.

The velocity dispersions in the end-states are also anisotropic. They are isotropic in the core where the orbits are well mixed, but become more radial at large radii. This is regardless of whether the initial orbits were isotropic or circular. There is a slight preference for the orbits to be more radial in the collision direction (this is presumably what maintains the flattened shape), but this is not marked except for f3fast. A typical profile of velocity dispersion anisotropy, $\beta = 1 - \sigma_t^2/\sigma_r^2$, where σ_r and σ_t are the diagonal components of the three-dimensional velocity dispersion tensor, is shown in Fig. 9. It is not well fitted by a function of the form $1 - r^2/r_c^2$, as is often assumed for analytical convenience.

To summarize this section, the merger products do seem to tend towards a unique profile which, for the simulations discussed here, resembles a de Vaucouleurs profile. This convergence is not perfect, and small differences remain which are dependent upon the merger history (impact parameter, collision speeds, etc.). The final haloes show various degrees of flattening, but all possess anisotropic velocity dispersions in their outer regions.

4 DISCUSSION

4.1 Scaling laws

For each density profile there is at least one characteristic radius, R, which is fixed by mass conservation. For $s < 3$, R is the outer radius; for $s > 3$ it is the inner, core radius, and when s varies from <3 in the centre to >3 in the outer regions (i.e. the de Vaucouleurs profile or something similar) it is the effective or half-light radius. We next look at how this characteristic radius changes in a merger, and check the results against our simulations.

Assuming a strict homology, $m \propto \rho(R)R^3$ and $e \propto m^2/R$. Therefore

$$\frac{R_f}{R_i} = \frac{2f_m^2}{f_e} \quad \text{and} \quad \frac{\rho(R_f)}{\rho(R_i)} = \frac{f_e^3}{4f_m^5}. \tag{6}$$

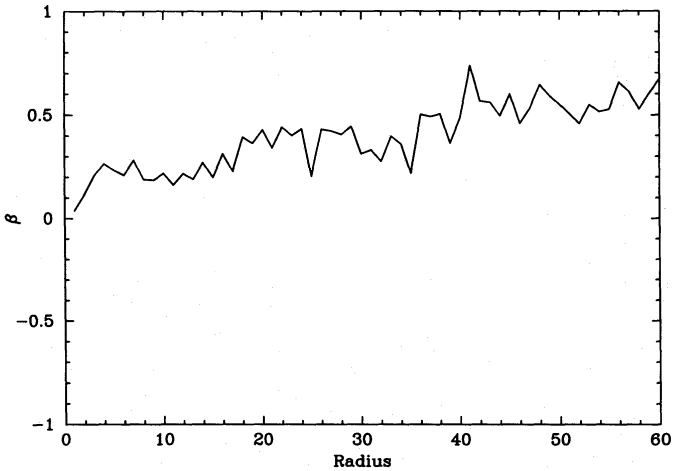

Figure 9. $\beta = 1 - \sigma_t^2/\sigma_r^2$ plotted against radius for the end-state of run f3.

The predicted half-mass radius (assuming a perfect homology) and the actual final value are shown in columns 9 and 8 of Table 1. Perhaps surprisingly, the predicted values are close to the measured ones in almost all cases. Where the initial conditions were close to the final profile and homologous growth is possible, the correspondence is particularly good. The biggest differences occur for the circular runs where the core structure undergoes a large change, concentrating many more particles into the central regions and reducing the half-mass radius.

We next consider how our merger-scaling arguments fit in with the usual cosmological ones (e.g. Kaiser 1986). These take into account the expected epoch of formation of particular masses $1 + z \propto \delta_0 \propto m^{-\alpha}$, where δ_0 is the characteristic root-mean-square density fluctuation on a mass-scale m, which is usually taken to be a power law with $0 \le \alpha \le \frac{2}{3}$. Then

$$R \propto m^{(1/3)+\alpha} \quad \text{and} \quad \rho \propto m^{-3\alpha}. \tag{7}$$

The two sets of scaling laws given by equations (6) and (7) agree when

$$\alpha = \frac{\ln(2f_m^2/f_e)}{\ln(2f_m)} - \frac{1}{3}. \tag{8}$$

If $f_m = f_e$, then $\alpha = \frac{2}{3}$, which corresponds to the greatest possible separation in redshift between different mass-scales. On the other hand, putting $\alpha = 0$ leads to $f_e^3 = 4f_m^5$, which implies $\rho(R_i) = \rho(R_f)$ from equation (6). This is as expected, because $\alpha = 0$ corresponds to equal fluctuations on all mass-scales, which therefore all collapse at the same time. Putting in typical values $f_e \approx 1.2$ and $f_m \approx 1.0$ from our simulations, we find that $\alpha \approx 0.4$. In the cold dark matter scenario our simulations would thus correspond to clusters of galaxies, whereas galaxies themselves correspond to smaller values of α. We would not expect a variation of α to alter our basic conclusion that an homology is attained with no inner core in the density profile.

4.2 The form of the homologue

The final density profile in our simulations resembles that of de Vaucouleurs. The precise form of the homologue may, however, be dependent upon the choice of initial conditions. It is known from collapse simulations that cold, clumpy initial distributions enable more efficient relaxation, and hence have more extended profiles than hotter, smoother ones (van Albada 1982; May & van Albada 1984; Aquilar & Merritt 1990; Katz 1991; Londrillo et al. 1991).

The theory of secondary infall considers the accretion of spherical shells of matter on to an existing spherically symmetric halo (Hoffman & Shaham 1985). This tends to give density profiles $\rho \propto r^{3(3+n)/(4+n)}$ with clusters having steeper profiles than galaxies, at least in the cold dark matter scenario.

Cosmological simulations tend to support the secondary infall picture. Note, however, that in most cases the number of particles per halo is small, and numerical relaxation is often a problem. The detailed form of the homology therefore awaits more accurate simulations.

4.3 X-ray luminosities of clusters of galaxies

The X-ray observations of the hot gas in clusters reveal resolved cores (Jones & Forman 1984). However, the interpretation of these observations is difficult, as the beam widths involved are not much less than the observed core radii, and many clusters have been shown by *ROSAT* data to have obvious X-ray substructure. The X-ray emission is dominated by the core. Suppose the gas to be isothermal and to have a density profile

$$\rho = \rho(R)\left(\frac{r}{R}\right)^{-s_x}. \tag{9}$$

Then $\mathrm{d}L \propto \rho^2 T^{1/2} 4\pi r^2 \mathrm{d}r \propto r^{3-2s_x}\,\mathrm{d}\,\log r$, which diverges to small radii for $s_x > \frac{3}{2}$. Therefore

$$L_x \propto \rho(r_x)^2 T^{1/2} r_x^3 \propto \rho(R)^2 T^{1/2} r_x^{3-2s_x} R^{2s_x} \propto m^{(1/3)-(13/2)\alpha} r_x^{3-2s_x} R^{2s_x}, \tag{10}$$

where r_x is the X-ray core radius. In a strict hierarchy in which r_x scales as R and in which $\rho \propto m^{-3\alpha}$, $T \propto m^{2/3-\alpha}$ and $R \propto m^{1/3+\alpha}$, we have $L_x \propto m^{4/3-7\alpha/2}$. The X-ray luminosity should be higher in the past for clusters for which $\alpha > \frac{8}{21}$. This is contradicted by observations (Edge et al. 1990; Henry et al. 1992) which show a strong increase in the number density of X-ray luminous clusters at low redshift.

The X-ray data are more consistent with a model in which the X-ray core radius remains constant as clusters evolve, as is the case in our full simulations (Edge et al. 1990; Pearce & Thomas 1991). We have argued, however, that the core radius of the dark matter should be negligible. Let us consider a model in which there is no inner core radius in the dark matter. Then one might expect that, as the sound crossing time for the gas is short compared to the dynamical time, the gas density should closely follow the general cluster profile. This would imply infinite X-ray emission from the centre. Indeed, this argument has been used in reverse to show that the presence of a gas core indicates a similar dark matter core. However, the high central X-ray luminosity leads to a cooling time in the centre of the cluster that is less than a Hubble time, and so a cooling flow will occur. The inflowing gas will have higher entropy, and so will have a lower density and longer cooling time; so an X-ray core radius will establish itself. The details of the flow are quite complicated. In the centre there will be a supersonic inflow of gas, as the cooling time is very short. Further out the flow will be subsonic, eventually merging on to the essentially hydrostatic pressure supported atmosphere. Let us suppose, however, that the X-ray luminosity is determined by the properties of the intracluster medium at the 'cooling radius' at which the cooling time is a Hubble time.

The cooling time, t_c, for bremsstrahlung radiation is $t_c \propto T^{1/2}/\rho$, where ρ is given by equation (9). We set t_c equal to a Hubble time ($\propto m^\alpha$) in order to determine the cooling radius, r_x:

$$r_x \propto m^{(1/3)+\alpha-(1/s_x)[(1/3)+(3/2)\alpha]}. \tag{11}$$

For clusters, $\alpha \approx 0.5$ and $s_x \approx 2$, which gives $r_x \propto m^{7/24}$ and $L_x \propto m^{1/8}$. Of course, this argument needs to be worked out in much more detail, but it does suggest that a core in the gravitational potential field is not required. Cooling can break the divergence of luminosity, while at the same time maintaining a positive luminosity evolution.

5 CONCLUSIONS

In this paper we are concerned with the morphology of dark matter haloes in hierarchical cosmologies in which the growth of structure under gravity is self-similar. This presupposes a fluctuation spectrum that is a pure power law (i.e. scale-free) and that is divergent to low masses. It is often supposed that galaxies and clusters form homologous families, i.e. that they all look the same apart from a scaling factor. We have investigated whether this is a reasonable assumption by simulating the formation of a halo by merging two smaller ones. The model we have used was deliberately kept simple to allow us to obtain precise answers to a particular problem and to enable us to see what was occurring. In this sense our model is unrealistic: it neglects mergers of three or more objects, of unequal-sized bodies and the accretion of intergalactic material. We feel, however, that our principal results will extend to more complicated situations.

In any hierarchy there must be some minimum mass (e.g. the Jeans mass) for collapsed objects. The structure of these first haloes need not correspond to that of the homologous family which establishes itself at late times. We choose to start with a density profile of the form given in equation (1), with the density slope, s, lying between 2 and 4. We find in all cases that it tends towards a value of 3, but is steeper at the outside (as it must be to ensure conservation of mass) and shallower in the middle. In this sense the de Vaucouleurs profile is a good approximation over much of the range, although we must necessarily have a finite phase-space density at the origin (Tremaine, Hénon & Lynden-Bell 1986). This profile is typical of many, but not all, previous simulations. It seems likely that the precise shape of the profile will depend upon the details of the formation process.

We find that in all our simulations the core radius shrinks by close to the maximum amount allowable under phase-space constraints. This has obvious implications for the formation of elliptical galaxies, but we suggest that it may be applicable to galaxy clusters also. It used to be thought that these had large core radii in the galaxy distribution, but recent observations suggest otherwise (e.g. Beers & Tonry 1986; Merrifield & Kent 1989). X-ray observations also show large cores. However, the central, dense gas is thought to be cooling on time-scales less than a Hubble time (Fabian, Nulsen & Canizares 1984), and the X-ray core may result from a taming of this divergence. The presence of a gas core does not imply an equivalent dark matter core.

We next intend to put hydrodynamics into these models, allowing us to follow the gas. This will allow us to test directly whether the gas becomes decoupled from the dark matter or whether it is an accurate tracer of the dark matter density profile (Pearce, Thomas & Couchman 1993).

ACKNOWLEDGMENTS

FRP was supported by a SERC studentship. PAT and HMPC acknowledge a NATO Collaborative Research Grant CR6920182 which facilitated their interaction. We acknowledge the facilities of the STARLINK minor node at Sussex.

REFERENCES

Aquilar L., Merritt D., 1990, ApJ, 354, 33
Barnes J., Hut P., 1986, Nat, 324, 446
Beers T. C., Tonry J. L., 1986, ApJ, 300, 557
Binney J., Tremaine S., 1987, Galactic Dynamics. Princeton Univ. Press, Princeton
Cavaliere A., Santangelo P., Tarquini G., Vittorio N., 1986, ApJ, 305, 651
Couchman H. M. P., 1991, ApJ, 368, L23
Edge A. C., Stewart G. C., Fabian A. C., Arnaud K. A., 1990, MNRAS, 245, 559
Efstathiou G. P., Frenk C. S., White S. D. M., Davis M., 1988, MNRAS, 235, 715
Evrard A. E., 1990, ApJ, 363, 349
Fabian A. C., Nulsen P. E. J., Canizares C. R., 1984, Nat, 310, 733
Henry J. P., Gioia I. M., Maccacaro T., Morris S. L., Stocke J. T., Wolter A., 1992, ApJ, 386, 408
Hernquist L., 1987, ApJS, 64, 715
Hoffman Y., Shaham J., 1985, ApJ, 297, 16
Jones C., Forman W., 1984, ApJ, 276, 38
Kaiser N., 1986, MNRAS, 222, 323
Katz N., 1991, ApJ, 368, 325
King I. R., 1966, AJ, 71, 64
Londrillo P., Messina A., Stiavelli M., 1991, MNRAS, 250, 54
May A., van Albada T. S., 1984, MNRAS, 209, 15
Merrifield M. E., Kent S. M., 1989, AJ, 98, 351
Merritt D., 1988, ASP Conf. Ser. Vol. 5, Minnesota Lectures on Clusters of Galaxies. Astron. Soc. Pac., San Francisco
Pearce F. R., Thomas P. A., 1991, MNRAS, 250, 607
Pearce F. R., Thomas P. A., Couchman H. M. P., 1993, preprint, Univ. Sussex
Press W. H. Schechter P., 1974, ApJ, 187, 425
Quinn T., Binney J., 1992, MNRAS, 255, 729
Quinn P. J., Salmon J. K., Zurek W. H., 1986, Nat, 322, 329
Thomas P. A., Couchman H. M. P., 1992, MNRAS, 257, 11
Tremaine S., Hénon M., Lynden-Bell D., 1986, MNRAS, 219, 285
van Albada T. S., 1982, MNRAS, 201, 939
Villumsen J. V., 1982, MNRAS, 199, 493
Villumsen J. V., 1983, MNRAS, 204, 219
Warren M. S., Quinn P. J., Salmon J. K., Zurek W. H., 1992, ApJ, 399, 405
West M. J., Dekel A., Oemler A., 1987, ApJ, 316, 1
White S. D. M., 1978, MNRAS, 184, 185
White S. D. M., 1979, MNRAS, 189, 831
White S. D. M., 1980, MNRAS, 191, 1P
Young P. J., 1976, AJ, 81, 807